A novel quasi-cubic CuFe2O4–Fe2O3 catalyst prepared at low temperature for enhanced oxidation of bisphenol A via peroxymonosulfate activation

Oh, Wen-Da; Dong, Zhili; Hu, Zhong-Ting; Lim, Teik-Thye

2015

Oh, W.-D., Dong, Z., Hu, Z.-T., & Lim, T.-T. (2015). A novel quasi-cubic CuFe2O4–Fe2O3 catalyst prepared at low temperature for enhanced oxidation of bisphenol A via peroxymonosulfate activation. Journal of Materials Chemistry A, 3(44), 22208-22217.

https://hdl.handle.net/10356/82691

https://doi.org/10.1039/C5TA06563A

Journal of Materials Chemistry A

Accepted Manuscript

This article can be cited before page numbers have been issued, to do this please use: W. Oh, Z. Dong, Z. Hu and T. Lim, *J. Mater. Chem. A*, 2015, DOI: 10.1039/C5TA06563A.

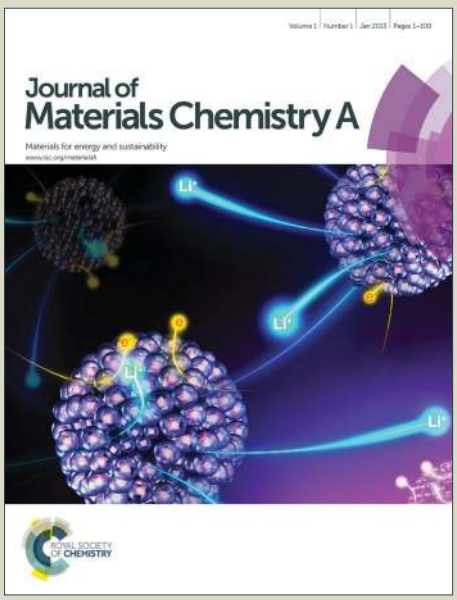

ROYAL SOCIETY OF CHEMISTRY

www.rsc.org/materialsA

View Article Online
DOI: 10.1039/C5TA06563A

Graphical Abstract

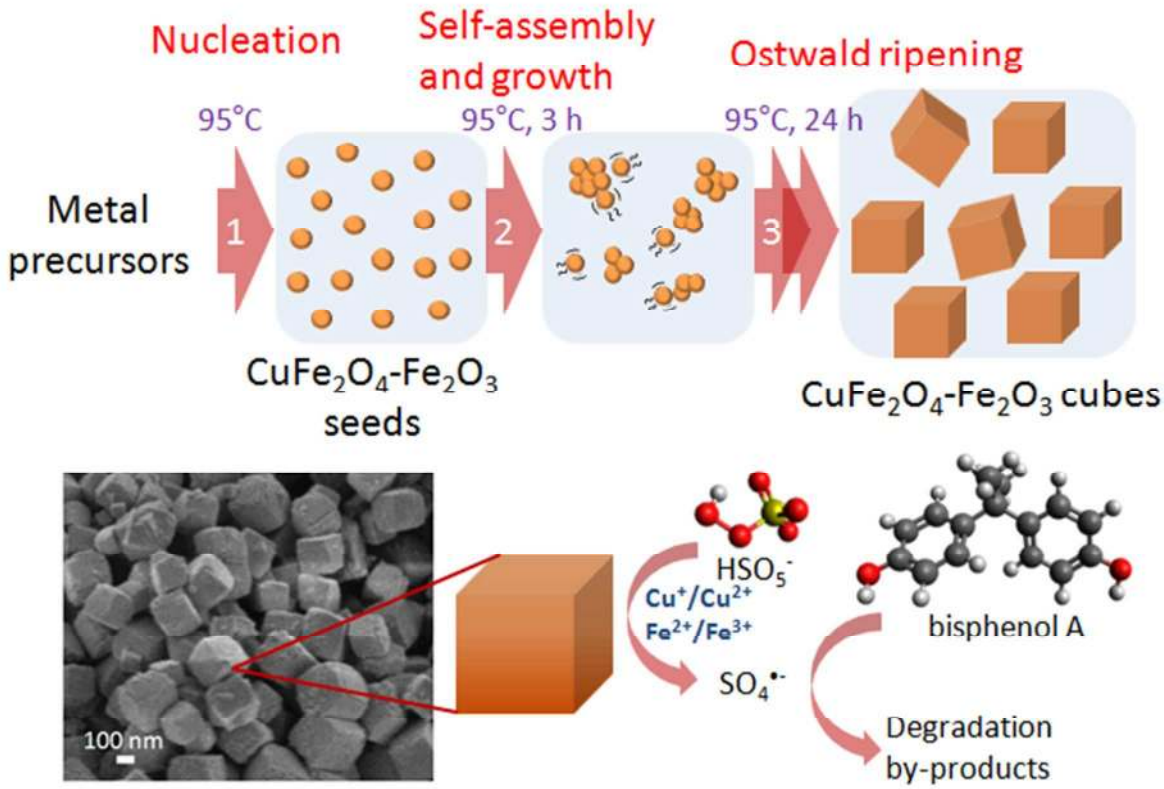

View Article Online
DOI: 10.1039/C5TA06563A

Journal Name

ARTICLE

A novel quasi-cubic $CuFe_2O_4$–Fe_2O_3 prepared at low temperature for enhanced oxidation of bisphenol A via peroxymonosulfate activation

Received 00th January 20xx,
Accepted 00th January 20xx

DOI: 10.1039/x0xx00000x

www.rsc.org/

Wen-Da Oh[a, b], Zhili Dong[a, c], Zhong-Ting Hu[b], Teik-Thye Lim[a, b]*

Abstract: A facile eco-friendly co-precipitation synthesis at low temperature was employed to fabricate $CuFe_2O_4$–Fe_2O_3 for the oxidation of bisphenol A (BPA) via peroxymonosulfate (PMS) activation. The formation mechanism of $CuFe_2O_4$–Fe_2O_3 at low temperature is proposed. The FESEM and BET characterization studies revealed that the $CuFe_2O_4$–Fe_2O_3 has a quasi-cubic morphology and specific surface area of 63 m^2 g^{-1}. The performance of $CuFe_2O_4$–Fe_2O_3 as a PMS activator was compared with other catalysts and the results indicated that the performance was in the following order: $CuFe_2O_4$–Fe_2O_3> $CuFe_2O_4$> $CoFe_2O_4$> $CuBi_2O_4$> $CuAl_2O_4$> Fe_2O_3>$MnFe_2O_4$. A kinetic model with mechanistic consideration of the influence of pH, PMS dosage and catalyst loading was developed to model the BPA degradation. The intrinsic rate constant (k_i) was obtained from the kinetic study. The relationship between the pseudo first-order rate constant and k_i was established. The trend of k_i revealed that increasing the catalyst loading decreased the BPA removal rate due to the initial preferential production of the weaker radicals (i.e. $SO_5^{\bullet-}$) for BPA degradation and Fe^{2+} quenching of $SO_4^{\bullet-}$ at higher catalyst loading. The influences of water matrix species (i.e. Cl^-, NO_3^-, HCO_3^-, PO_4^{3-} and humic acid) on BPA degradation rate were also investigated. The $CuFe_2O_4$–Fe_2O_3 catalyst exhibited excellent stability and can be reused for at least several times without significant deterioration in performance.

1. Introduction

Advanced oxidation processes utilizing redox change in transition metals are extensively used for catalytic oxidation of organic pollutants. Oxidation of organic pollutant by sulfate radical generated from the redox reaction between commercially-available oxidant and transition metals is increasingly adopted as an eco-friendly and efficient method for removing recalcitrant pollutants in water. Sulfate radical has a relatively high oxidation potential (E_o = 2.7 V) and it is selective for electron transfer reaction [1]. Sulfate radical has a longer half-life compared to the hydroxyl radical thus allowing better diffusion of the generated reactive sulfate radical for oxidation reactions in the bulk solution [2]. One of the most efficient ways to generate sulfate radical is by peroxymonosulfate (PMS) activation using transition metals which can be achieved in both heterogeneous and homogeneous reaction systems [3]. The heterogeneous system is advantageous over the homogeneous system due to the ease of recovering the catalyst for further reuse and prevention of water pollution by the added metals. Current trend of study involves the use of Co-based materials as PMS activators but this approach suffers from the dissolution of highly-toxic Co ions during treatment [4, 5]. One appealing transition metal which is relatively less toxic than Co is Cu. To date, the Cu-based catalysts which have been reported include $CuFe_2O_4$ [6, 7], CuO [8] and Cu/ZSM5 [9]. In most cases, the catalyst preparation method involves high-temperature heat treatment, environmentally-harmful solvents and other organic precursors. For pragmatic application, a facile low-energy and eco-friendly synthesis is warranted.

Bisphenol A (BPA) is a xenobiotic endocrine disruptor ubiquitously used in various manufacturing industries to produce polycarbonate plastics and epoxy resins [10]. Due to its endocrine distrupting property and widespread application, pollution due to BPA poses a potential risk to human health and aquatic lives [11, 12]. Although a myriad of treatment methods has been proposed in the literature such as ozonation and activated carbon adsorption, these methods require high energy consumption or generate secondary waste stream [13].

Previous investigation of the kinetics of pollutant oxidation by sulfate radical in the heterogeneous system often based on the pseudo first-order kinetics with the assumption that the

[a]Nanyang Environment and Water Research Institute (NEWRI), Interdisciplinary Graduate School (IGS), Nanyang Technological University, 1 Cleantech Loop, CleanTech One, Singapore 637141, Singapore.
[b]Division of Environmental and Water Resources Engineering, School of Civil and Environmental Engineering, Nanyang Technological University, 50 Nanyang Avenue, Singapore 639798, Singapore.
[c]School of Materials Science and Engineering, Nanyang Technological University, 50 Nanyang Avenue, Singapore 639798, Singapore.
*Corresponding author. Tel: +65-6790 6933, Fax: +65-6791 0676,
E-mail address: cttlim@ntu.edu.sg (Lim T.T.)
Electronic Supplementary Information (ESI) available: [details of any supplementary information available should be included here]. See DOI: 10.1039/x0xx00000x

oxidant (PMS) added was readily available for reaction [14, 15]. Qi et al. presented a second-order kinetic model to describe the degradation of caffeine by Co-MCM41 catalyst [16]. However, these kinetic models did not take into account the influence of pH, PMS dosage and catalyst loading on pollutant degradation particularly under non-ideal conditions (e.g. non-excess PMS, different pHs, etc.). In this regard, a more robust kinetic model needs to be employed.

Herein, the objectives of this study are to (i) prepare and characterize a series of catalysts encompassing of $CuFe_2O_4$–Fe_2O_3, ferrospinels (YFe_2O_4, Y = Cu, Co and Mn), Cu-based spinels (CuX_2O_4, X = Bi and Al) and Fe_2O_3, (ii) investigate and compare the performance of the as-prepared catalysts for BPA removal via PMS activation, and (iii) develop a kinetic model based on the mechanistic consideration of various influencing parameters (i.e. pH, PMS dosage and catalyst loading) to describe the BPA degradation. The intrinsic rate constant, k_i, was calculated explicitly from the experimentally-derived BPA degradation at various time intervals in the kinetic modelling study and it was compared with the pseudo first-order rate constant (k_{app}) to obtain new insights into the use of heterogeneous transition metal catalyst for pollutant removal via PMS activation.

2. Experimental

2.1 Chemicals

All the chemicals used in this study are of analytical grade. The chemicals used are as follow: $Cu(NO_3)_2{\cdot}3H_2O$ (QrëC), $Co(NO_3)_2{\cdot}6H_2O$ (Alfa Aesar), $Mn(NO_3)_2{\cdot}4H_2O$ (Sigma-Aldrich), $Fe(NO_3)_3{\cdot}9H_2O$ (Merck), $Bi(NO_3)_3{\cdot}5H_2O$ (Alfa Aesar), $Al(NO_3)_3{\cdot}9H_2O$ (Sigma-Aldrich), NaOH (Alfa Aesar), HCl (Merck), acetonitrile (Merck), citric acid (Merck), ammonia (Hach), KI (Fisons), PMS (in the form of Oxone®, $2KHSO_5{\cdot}KHSO_4{\cdot}K_2SO_4$, Alfa Aesar), NaCl (Qrëc™), $NaNO_3$(Sigma–Aldrich), humic acid (HA, Aldrich), $NaHCO_3$ (Sigma–Aldrich), polyethylene glycol (Sigma–Aldrich), sodium acetate (Sigma-Aldrich), bisphenol A (Merck) and methanol (Merck). All the experiments were conducted using deionized (DI) water (18.2 MΩ cm).

2.2 Synthesis of catalysts

The $CuFe_2O_4$–Fe_2O_3 catalyst was prepared using a facile co-precipitation method at low temperature. In a typical synthesis procedure, metal precursors consisting of 5 mmol of $Cu(NO_3)_2{\cdot}3H_2O$ and 10 mmol of $Fe(NO_3)_3{\cdot}9H_2O$ were dissolved in 50 mL of DI water and pH of the solution mixture was adjusted to pH 10-11 using 6 M NaOH under rapid magnetic stirring. Then, the resultant solution was heated under vigorous stirring at 95°C for 24 h to promote hydrolysis and the formation of $CuFe_2O_4$–Fe_2O_3 catalyst. The resultant brownish product was separated from the solution by a simple magnetic separation procedure and freeze-dried for 24 h. Several other catalysts, namely $CuAl_2O_4$, $CuBi_2O_4$, $CuFe_2O_4$, $MnFe_2O_4$, $CoFe_2O_4$ and Fe_2O_3 were also prepared for performance comparison with $CuFe_2O_4$–Fe_2O_3. The $CuAl_2O_4$ was prepared via a sol-gel method [17]. The $CuBi_2O_4$ and Fe_2O_3 were prepared via a low-temperature co-precipitation method [13]. The XFe_2O_4 (X = Mn, Fe and Co) was prepared via a solvothermal method [18]. The details of the synthesis procedures for preparing ferrospinels (YFe_2O_4, Y = Cu, Co and Mn), Cu-based spinels (CuX_2O_4, X = Bi and Al) and Fe_2O_3 are presented in the Supplementary Materials.

2.3 Characterization technique

The crystallographic and mineralogical information of the as-prepared catalysts were obtained using a X-ray diffractometer (Bruker AXS D8 Advance) operated at 40 kV and 40 mA with a Cu-Kα (λ = 1.5418 Å) X-ray source. The surface morphology and EDX elemental distribution were studied by obtaining the electron micrographs and elemental mappings using a field emission scanning electron microscopy (FESEM, JEOL JSM-7600F) equipped with a energy dispersive X-ray spectroscope (EDX, Oxford Xmax80 LN_2 Free). The Fourier transform infrared (FTIR) spectra were obtained using a FTIR spectrometer (Perkin Elmer Spectrum GX). The Brunauer–Emmett–Teller (BET) specific surface area of the catalysts was calculated from the N_2 adsorption–desorption isotherm analysis at 77 K (Quantachrome Autosorb-1 Analyzer).

2.4 Performance evaluation

Batch experiment was conducted to investigate the performance of the catalyst for BPA treatment via PMS activation. In a typical experimental procedure, a known amount of PMS was introduced into the reaction vessels containing 100 mL of 5 mg L^{-1} of BPA at 25°C. The pH of the solution was immediately adjusted to the desired pH (pH 4.5, 7.0 or 9.5). Then, a known amount of the catalyst was added into the solution to commence the catalytic reaction. At various time intervals, 2-mL aliquot was sampled from the reaction vessel to determine the BPA concentration. The collected aliquot was filtered using a cellulose acetate membrane filter and the catalytic reaction was quenched using methanol. The BPA concentration was then determined using a high performance liquid chromatography (HPLC). At the end of the reaction time, the pH change of the solution at pH 4.5 was insignificant while for pH 7.0 and 9.5, the final pH were 6.1 and 8.1, respectively, due to their unbuffered condition and the formation of acidic BPA intermediates such as organic acid [13]. The experimental parameters studied were the PMS dosage (0.18, 0.27 and 0.36 g L^{-1}), catalyst loading (0.05, 0.10 and 0.20 g L^{-1}) and initial pH (4.5, 7.0 and 9.5). The mol ratio of PMS to pollutant used in this study was comparable to other study [19]. At the end of the reaction time, the total organic carbon and Cu leaching was also determined for selected conditions. For the TOC determination, the samples were filtered and analyzed immediately without quenching with methanol. Investigation of the changes in PMS concentration over time was also conducted.

2.5 Analytical methods

The BPA concentration was determined from the calibration curve which was developed using a HPLC (Perkin Elmer, UV detector) operated with a reverse phase column (Hypersil Gold) and a mobile phase consisting of 60% acetonitrile to 40% water. The BPA detection wavelength was

220 nm. TOC and Cu ion measurements were conducted using a TOC Analyzer (Shimadzu ASI-V) and ICP-OES (PerkinElmer, Elmer Optima 2000DV), respectively. The point of zero charge (pH_{zpc}) of the catalyst was determined using the pH drift method as described by Lopez-Ramon et al. [20] with slight modification. Briefly, a series of 30 mL of 0.01 mM of NaCl solution was prepared. Then, 0.09 g of the catalyst was added into the solutions and the pH of the solutions was adjusted to between pH 3-12 using 1 M NaOH or 0.1 M HCl. After 48 h, the pH of the solutions was measured again and the pH_{zpc} which is the point of which pH(initial) = pH(final) was determined from the intercept of ΔpH vs. pH(initial) plot. The PMS concentration was quantified using the iodometric method with the aid of a UV-Vis spectrophotometer. Briefly, 5 mL of sample was mixed with 1 g of KI and agitated vigorously for 30 min. Then, the sample mixture was analyzed using a UV-Vis spectrophotometer at λ_{max} = 353 nm and the PMS concentration were determined using a pre-developed calibration curve.

3. Results and discussions

3.1 Synthesis and characteristics of the as-prepared catalysts

The $CuFe_2O_4$–Fe_2O_3 catalyst was successfully prepared by employing an eco-friendly solvent- and surfactant-free co-precipitation method at low temperature. The low temperature synthesis method was previously used to prepare Fe_2O_3 [13]. The $CuFe_2O_4$–Fe_2O_3 presents an improvement over the Fe_2O_3 catalyst due to the presence of Cu which can lead to the synergistic Cu and Fe coupling effect. For performance comparison, other catalysts, namely ferrospinels (YFe_2O_4, Y = Cu, Co and Mn), Cu-based spinels (CuX_2O_4, X = Bi and Al) and Fe_2O_3, were also prepared using various synthesis methods encompassing solvothermal, sol-gel, hydrothermal and co-precipitation methods. Fig. 1(a) shows the XRD patterns and FTIR spectra of all the as-prepared catalysts. The XRD peaks of the $CuFe_2O_4$–Fe_2O_3 catalyst can be indexed to both $CuFe_2O_4$ spinel and Fe_2O_3 phases. Rietveld refinement analysis shows that the $CuFe_2O_4$–Fe_2O_3 catalyst has a compositional ratio (w/w) of 2 $CuFe_2O_4$ to 3 Fe_2O_3 (83% Fe^{3+}, 17% Cu^{2+}). All the solvothermally-prepared ferrospinels are of single phase except for $CuFe_2O_4$ which has 20% w/w of Cu^0 attributed to the use of ethylene glycol which can act as a reducing agent [21]. The XRD pattern of $CuBi_2O_4$ can be indexed to the single phase $CuBi_2O_4$. The XRD pattern of $CuAl_2O_4$ shows that additional peaks attributed to a small amount of CuO (~10% w/w by Rietveld refinement analysis) are also present. In all the FTIR spectra (Fig. 1b), the broad band located at ~3400 cm^{-1} is indicative of the presence of surface hydroxyl functional groups. The surface hydroxyl group is partly responsible for enhancing the pollutant oxidation rate [22, 23]. The distinctive peak at 600 cm^{-1} in all the FTIR spectra was the characteristic Me-O bond.

The FESEM micrograph (Fig. 2d) of $CuFe_2O_4$–Fe_2O_3 catalyst consists of quasi-cubic morphology with mean size of 100-200 nm. The EDX elemental mapping (Fig. 2e) shows that Cu and Fe

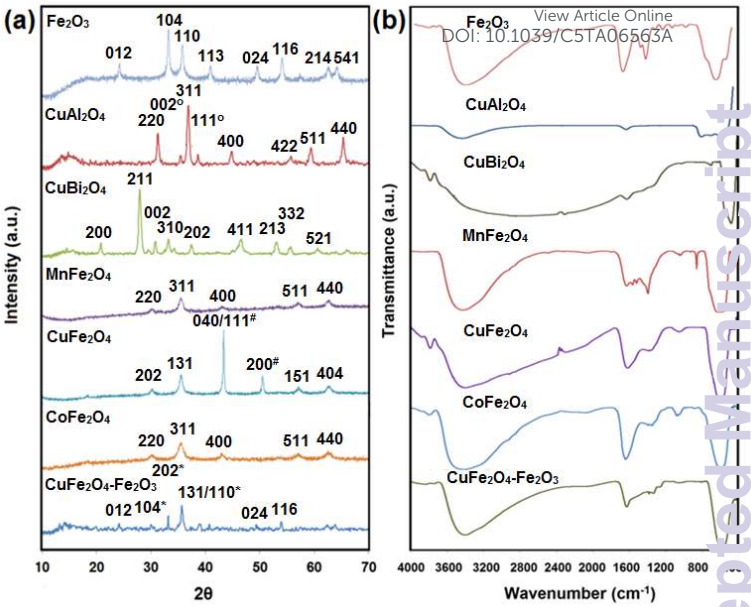

Fig. 1: XRD patterns (a) and FTIR spectra (b) of the as-prepared catalysts. * = Fe_2O_3, # = Cu and ° = CuO.

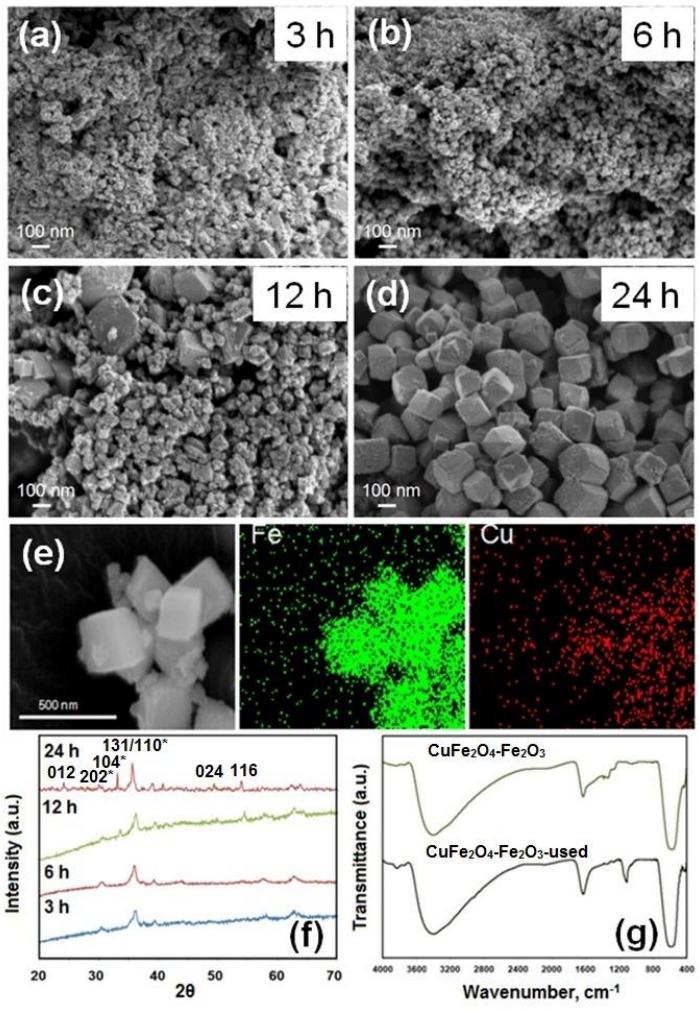

Fig. 2: (a-d) Time dependent FESEM micrographs, (e) EDX elemental mappings, (f) time-dependent XRD patterns, and (g) pristine and used FTIR spectra of $CuFe_2O_4$-Fe_2O_3 catalyst.

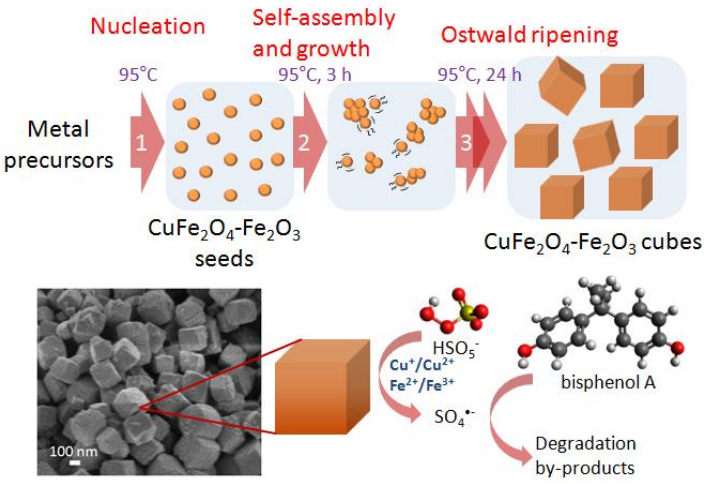

Fig. 3: Schematic illustration of the low temperature $CuFe_2O_4$–Fe_2O_3 synthesis protocol. Nucleation of the $CuFe_2O_4$-Fe_2O_3 occurs when the metal precursor was subjected to 95°C under basic condition. The $CuFe_2O_4$-Fe_2O_3 nucleus proceeds to grow and self-assemble to form cubic microstructure.

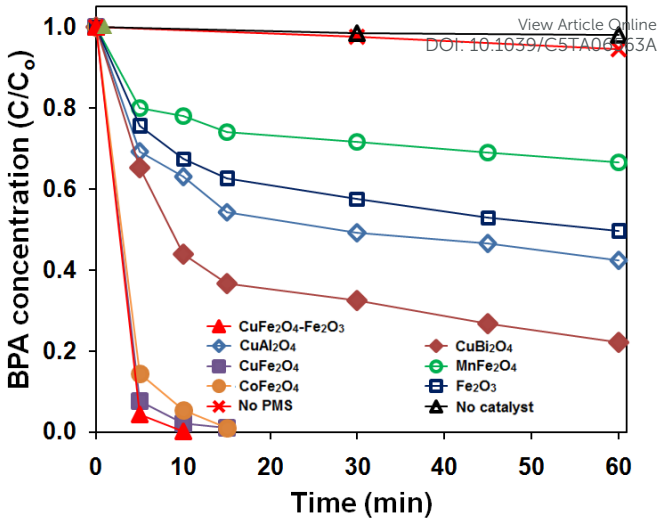

Fig. 4: BPA degradation curves for different catalysts. Initial conditions: [pH] = 7.0±0.2, [PMS] = 0.36 g L^{-1}, [catalyst] = 0.2 g L^{-1}, and [BPA] = 5 mg L^{-1}.

were homogeneously distributed on the surface at the ratio of 1 Cu to 5.5 Fe which is close to the theoretical ratio of 1 Cu to5 Fe. This indicates the coexistence of $CuFe_2O_4$ and Fe_2O_3 phases in the cubic nanostructure. The BET result indicates that it has a specific surface area of 63 m^2 g^{-1}. As the synthesis of spinel $CuFe_2O_4$ was carried out at a relatively lower synthesis temperature than those reported in the literature, the elapsed-aging time was crucial for obtaining the desired morphology and crystallographic phase [6, 7, 24]. To obtain insights to the formation of $CuFe_2O_4$–Fe_2O_3, the time-dependent FESEM micrographs and XRD patterns of $CuFe_2O_4$–Fe_2O_3 were obtained (Fig. 2). Although the catalysts prepared at t = 3 and 5 h has magnetic property, the FESEM micrograph and XRD pattern indicate that it consists of relatively amorphous nanoparticles. By further increase in the reaction time, the crystallinity of the nanoparticles improved and the nanoparticles began to self-assemble forming quasi-cubic structure via Ostwald ripening as indicated in Fig. 2c. The increase in synthesis time for the low temperature synthesis has also been reported to increase the crystallinity of a material [25]. The proposed schematic illustration of the $CuFe_2O_4$–Fe_2O_3 formation mechanism is shown in Fig. 3.

All the other catalysts were of quasi-spherical morphology (Fig. S1a-e) except for $CuAl_2O_4$ which consists of irregular microparticles (Fig. S1f). The solvothermal synthesis protocol involving the use of surfactant resulted in materials with relatively higher specific surface area than the low temperature co-precipitation method due to the significant reduction in agglomeration of the materials prepared with surfactant [26]. However, this occurs at the expenses of possible environmental pollution due to surfactant leaching during application (if the surfactant is not removed) and higher production cost. The low temperature co-precipitation method produces Fe_2O_3 with high surface area due to the employment of dipicolinic acid (DPA) for synthesis control [13]. However, $CuFe_2O_4$–Fe_2O_3 could not be formed in the presence of DPA possibly due to the complexation of Cu with DPA making it less available for reaction.

3.2 Performance evaluation

3.2.1 Comparison of various catalysts

Fig. 4 shows the performance comparison of various catalysts, namely $CuFe_2O_4$–Fe_2O_3, Fe_2O_3, CuX_2O_4 (X = Fe, Bi and Al) and YFe_2O_4 (Y = Cu, Co and Mn) for BPA degradation via PMS activation at various time intervals while Table 1 shows the BET specific surface area, TOC removal, first-order rate constant (k_{app}) and Cu leaching for various catalysts. The catalysts were compared with respect to different synthesis methods (i.e. solvothermal $CuFe_2O_4$ vs. low temperature co-precipitation $CuFe_2O_4$) and different mixed metal oxide systems (i.e. CuX_2O_4 (X = Fe, Bi and Al) and YFe_2O_4 (Y = Cu, Co and Mn)). The metal oxide catalysts contain transition metal (Me^{n+}) which can activate PMS to produce $SO_4^{\bullet-}$ for degrading BPA through the following single electron transfer reaction:

$Me^{n+} + HSO_5^- \rightarrow Me^{(n+1)+} + SO_4^{\bullet-} + OH^-$ (1)

$Me^{(n+1)+} + HSO_5^- \rightarrow Me^{n+} + SO_5^{\bullet-} + H^+$ (2)

$SO_4^{\bullet-} + BPA \rightarrow$ degradation by-products (3)

There was no significant BPA removal (<5% in 30 min) by adsorption and PMS oxidation. The performance of $CuFe_2O_4$–Fe_2O_3 catalyst synthesized at 3, 6 and 12 h was almost the same to that of 24 h (Fig. S2a). However, the $CuFe_2O_4$–Fe_2O_3 synthesized at 24 h was selected for further performance evaluation as it is relatively more stable (less amorphous) with homogeneous morphology compared with the others. Several other PMS dosages were also investigated prior to the performance comparison study (Fig. S2b). The activities of the catalysts are in the following order: $CuFe_2O_4$–Fe_2O_3> $CuFe_2O_4$> $CoFe_2O_4$> $CuBi_2O_4$> $CuAl_2O_4$> Fe_2O_3>$MnFe_2O_4$. The $CuFe_2O_4$–Fe_2O_3 catalyst performed better than all the other catalysts attributed to several factors, namely (i) its eco-friendly preparation method without using any organic precursor/solvent whose residue remaining in the resulting catalyst could reduce its catalytic activity, and (ii) efficient

Table 1: Synthesis method, BET specific surface area, TOC removal efficiency, Cu leaching and pseudo first-order rate constant (k_{app}) values for various catalysts.

Catalyst	Synthesis method	Specific surface area (m2 g-1)	TOC removal efficiency at 30 min (%)	Cu leaching (mg L-1)	kapp
$CuFe_2O_4$–Fe_2O_3	low-temperature co-precipitation	63	24 (52)*	0.9 (<0.1%)	0.62±0.04
$CuFe_2O_4$	solvothermal	101	-23	0.7 (<0.1%)	0.52±0.02
$CuBi_2O_4$	low temperature co-precipitation	9	15	0.6 (<0.1%)	0.08±0.01
$CuAl_2O_4$	sol-gel	39	13	0.2 (<0.1%)	0.07±0.00
$MnFe_2O_4$	solvothermal	151	-12	-	0.04±0.00
$CoFe_2O_4$	solvothermal	139	-32	-	0.38±0.01
Fe_2O_3	low-temperature co-precipitation	188	11	-	0.05±0.00

(*) indicates TOC removal at t = 6 h.

synergistic Cu and Fe redox coupling in the metal oxide framework which has a promotional effect on the PMS activation [7, 22, 24]. The TOC removal efficiency for $CuFe_2O_4$–Fe_2O_3 was 24% but by prolonging the reaction time to 6 h, the TOC removal efficiency increased to 52%. The use of organic precursor/solvent (i.e. surfactant) for synthesis could result in having surface-bound organics which are difficult to remove without using extreme heat treatment. These surface-bound organics could compete for reaction with $SO_4^{\bullet-}$ and prevent the effective utilization of generated radicals for pollutant degradation. This phenomenon explains the lower catalytic performance of the solvothermally-prepared $CuFe_2O_4$ and $CoFe_2O_4$ (k_{app} = 0.52±0.02 and 0.38±0.01, respectively) compared with the $CuFe_2O_4$–Fe_2O_3 catalyst despite having higher surface area for catalysis. In addition, the degradation of the surface-bound organics has the tendency of causing unfavourable TOC leaching which explains the observed negative TOC removal efficiencies when the $CuFe_2O_4$, $CoFe_2O_4$ and $MnFe_2O_4$ prepared by solvothermal method were employed as the catalyst for BPA treatment.

The redox transition between Cu^{2+}-Cu^{+}-Cu^{2+} in the presence of PMS yields both $SO_5^{\bullet-}$ and $SO_4^{\bullet-}$. Compared to Cu^{2+}, the Cu^{+} species, is relatively unstable and can be easily scavenged (e.g. by the dissolved oxygen). Considering the thermodynamic feasibility of the following reaction: $Cu^{+} + Fe^{3+} \rightarrow Cu^{2+} + Fe^{2+}$ (E_o = +0.60 V), the Fe^{3+} species acts as an intermediate electron acceptor and reduces the amount of Cu^{+} scavenged. In this regards, the $CuFe_2O_4$–Fe_2O_3 catalyst has an advantage over $CuFe_2O_4$ by having higher amount of Fe^{3+} which could decrease Cu^{+} scavenging and maximize the production of $SO_4^{\bullet-}$ thus enhancing the BPA degradation rate.

Since Cu^{2+} is the active species in $CuFe_2O_4$–Fe_2O_3 catalyst for PMS activation, the Cu leaching for all the Cu catalysts was compared. The Cu leaching during PMS activation of $CuFe_2O_4$–Fe_2O_3 catalyst was comparable with the solvothermally-

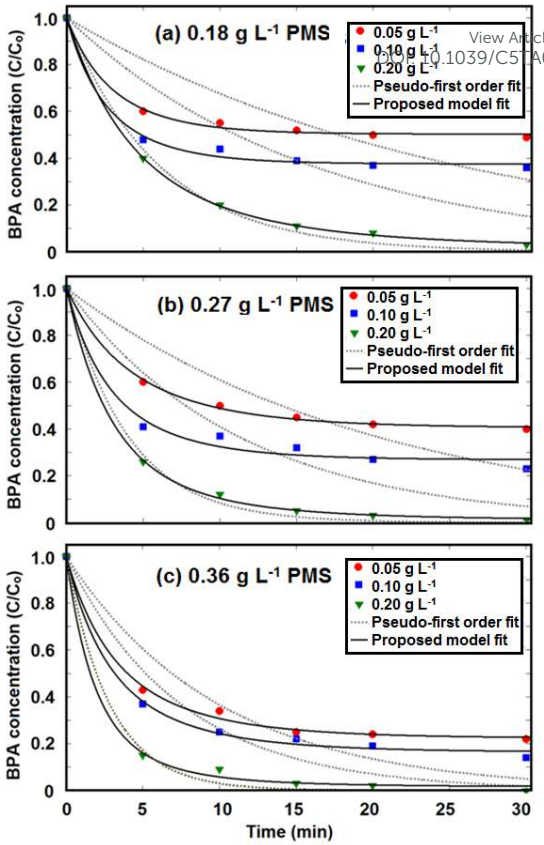

Fig. 5: Experimental and calculated BPA degradation curves for different PMS dosages at various catalyst loadings. Initial conditions: [pH] = 4.5±0.2 and [BPA] = 5 mg L^{-1}.

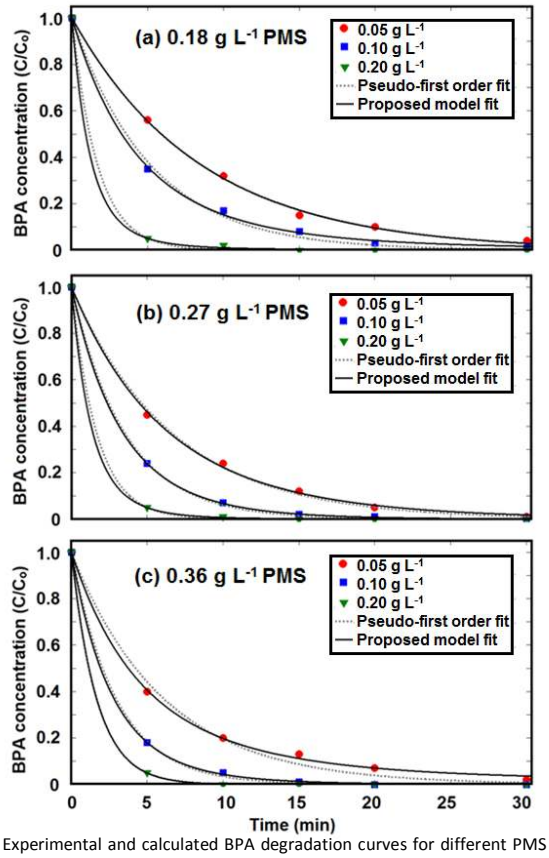

Fig. 6: Experimental and calculated BPA degradation curves for different PMS dosages at various catalyst loadings. Initial conditions: [pH] = 7.0±0.2 and [BPA] = 5 mg L^{-1}.

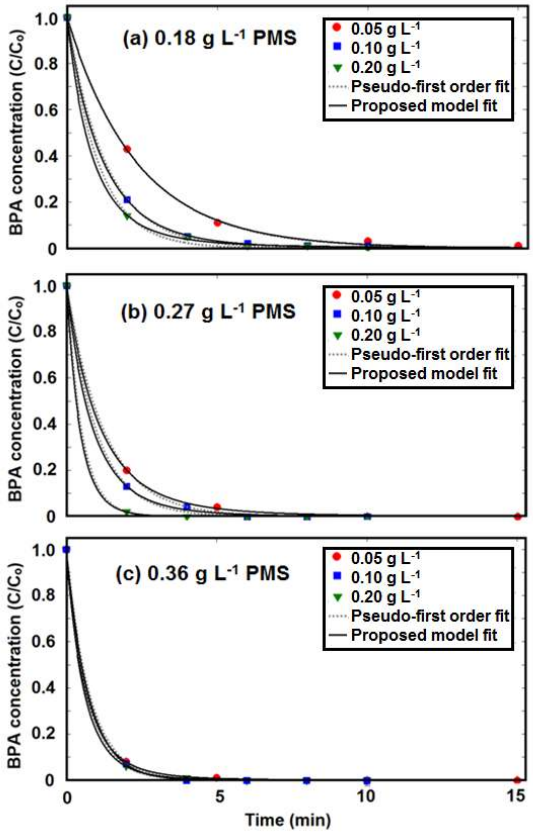

Fig. 7: Experimental and calculated BPA degradation curves for different PMS dosages at various catalyst loadings. Initial conditions: [pH] = 9.5±0.2 and [BPA] = 5 mg L^{-1}.

prepared $CuFe_2O_4$ ferrospinel (0.9 mg L^{-1} or 0.05 % vs. 0.7 mg L^{-1} or 0.04%, respectively). However, the $CuFe_2O_4$–Fe_2O_3 catalyst prepared with 3 h synthesis time exhibited 15.3 mg L^{-1} of Cu leaching or ~1% of the total catalyst weight loss further indicating that a relatively longer preparation time of 24 h is necessary to improve the crystallinity and stability of $CuFe_2O_4$–Fe_2O_3 catalyst for low temperature synthesis of the catalyst.

3.2.2 Effects of pH, catalyst loading and PMS dosage

Figs. 5-7 show the influence of several key parameters, namely the pH, PMS dosage and catalyst loading on BPA removal. The pH_{zpc} of $CuFe_2O_4$–Fe_2O_3 is determined to be pH 7.6 (Fig. S2c). Generally, the removal efficiency and rate improved with increasing pH, PMS dosages and catalyst loading. The pseudo-first order kinetics was employed to model the BPA degradation rate and the calculated pseudo first-order rate constant (k_{app}) at different conditions is presented in Table 2. While the pseudo first-order fittings at pHs 7.0 and 9.5 are generally good (R^2 > 0.9), the fitting at pH 4.5 is relatively poorer attributed to the oversimplification of the kinetic model which adopts a "black-box" approach. The pseudo first-order kinetics did not take into account the change of catalyst surface charge (Eq. (4)) and possible attachment of the protons to the more electronegative peroxide bond of the PMS molecule (Eq. (5)) at acidic pH which gives rise to the interfacial repulsion leading to the weaker catalytic performance [13]:

$$[Cat-OH] + H^+ \leftrightarrow [Cat-OH_2^+] \quad (4)$$

$$SO_2\text{-O-O-H} + H^+ \rightarrow SO_2\text{-O-O-}H_2^+ \quad (5)$$

where [Cat-OH] and [Cat-OH_2^+] are the densities of active and deactivated catalytic sites, respectively. The catalyst surface contains many surface hydroxyl moieties which is important for PMS activation and surface protonation influences the density of surface hydroxyl moiety. The effect was particularly more pronounced at lower catalyst loading and PMS dosage.

To address the limitation of the pseudo first-order kinetics, a kinetic model based on the mechanistic consideration that the catalytic sites could be partially deactivated as a result of surface protonation is adopted in this study. At equilibrium condition, the thermodynamic equilibrium constant (K_{eq}) for Eq. (4) can be expressed as follows:

$$K_{eq} = \frac{[Cat-OH]_o - [Cat-OH]}{[H^+][Cat-OH]} \quad (6)$$

where $[Cat\text{-}OH]_o$ is the catalyst loading. By incorporating the variables consisting of the catalyst loading and PMS dosage into the kinetic model, the rate of BPA removal can be given as follows:

$$\frac{dC_{BPA}}{dt} = -k_i[Cat-OH]C_{BPA}C_{PMS} \quad (7)$$

where C_{BPA} and C_{PMS} are the concentrations of BPA and PMS, respectively, and k_i is the intrinsic reaction rate constant. Considering that the changes of the C_{PMS} follows the first-order kinetics (Fig. S3) and by incorporating Eq. (6) into Eq. (7), the kinetic model can be further simplified as follows:

$$\frac{dC_{BPA}}{dt} = -k_i\frac{[Cat-OH]_o}{(K_{eq}[H^+]+1)}C_{BPA}C_{PMSo}e^{-k_{PMS}t} \quad (8)$$

where k_{PMS} is the first-order rate constant for PMS consumption. Eq. (8) can be solved analytically to become Eq. (9) by integrating with respect to t under the following boundary conditions: at t = 0, $C_{BPA} = C_{BPAo}$.

$$C_{BPA} = C_{BPAo}e^{\frac{k_i}{k_{PMS}}\frac{[Cat-OH]_o}{(Keq[H^+]+1)}C_{PMSo}(e^{-k_2t}-1)} \quad (9)$$

Eq. (9) will be explicitly validated by fitting with the experimental-obtained BPA degradation results using Matlab and the kinetic parameters can be calculated by optimization using the nonlinear least square method. Preliminary fittings indicated that all the K_{eq} have the value close to 1.0. The K_{eq} = 1 indicates that neither the [Cat-OH_2^+] and [Cat-OH] are favoured species and the equilibrium is dependent on pH (i.e.: when $[H^+]$ is higher at acidic pH, the [Cat-OH_2^+]/[Cat-OH] is higher). Therefore, K_{eq} was used as a constant for subsequent kinetic modelling study.

Table 2 also shows the calculated kinetic parameters consisting of k_i and k_{PMS} with their respective R^2. When the PMS is readily available for activation without significant influence by the pH (first-order), the relationship between k_{app} and k_i can be established by the following equation:

$$k_t = \frac{k_{app}(K_{eq}[H^+]+1)}{[Cat-OH]_o[PMS]_o} \quad (10)$$

A relatively good fit was observed for all cases (R^2>0.99) indicating that the kinetic model is able to account for the effect of different reaction pHs. In general, the trend of k_i value decreases linearly with increasing catalyst loading suggesting that the BPA oxidation reaction per unit catalyst

ROYAL SOCIETY OF CHEMISTRY View Article Online
DOI: 10.1039/C5TA06563A

Journal Name

ARTICLE

Table 2: Kinetic parameters of $CuFe_2O_4$–Fe_2O_3 catalyzed BPA degradation via PMS activation at various conditions.

PMS dosage (g L^{-1})	Catalyst loading (g L^{-1})	k_{app}	R^2	k_i	k_{PMS}	R^2
pH 4.5						
0.18	0.05	0.031±0.002	0.19	6.07±1.25	0.22±0.04	0.996
	0.10	0.046±0.001	0.21	4.85±0.50	0.23±0.03	0.991
	0.20	0.13±0.01	0.95	2.15±0.15	0.050±0.003	0.999
0.27	0.05	0.043±0.003	0.47	3.85±0.07	0.15±0.01	0.998
	0.10	0.062±0.001	0.49	3.27±0.18	0.19±0.01	0.985
	0.20	0.17±0.01	0.83	2.13±0.08	0.07±0.01	0.999
0.36	0.05	0.067±0.001	0.49	4.59±0.06	0.15±0.00	0.997
	0.10	0.083±0.003	0.59	2.71±0.06	0.15±0.01	0.995
	0.20	0.23±0.02	0.90	1.98±0.04	0.06±0.02	0.996
pH 7.0						
0.18	0.05	0.11±0.01	0.99	4.98±0.41	0.02±0.01	0.996
	0.10	0.16±0.01	0.99	4.68±0.29	0.04±0.01	0.999
	0.20	0.46±0.04	0.98	4.13±0.18	0.004±0.002	0.999
0.27	0.05	0.14±0.01	0.96	4.18±0.10	0.016±0.002	0.999
	0.10	0.24±0.01	0.98	4.03±0.02	0.03±0.01	0.999
	0.20	0.53±0.07	0.91	5.43±0.10	0.11±0.02	0.999
0.36	0.05	0.14±0.01	0.90	4.16±0.20	0.043±0.001	0.999
	0.10	0.28±0.04	0.96	3.98±0.33	0.05±0.01	0.999
	0.20	0.62±0.04	0.99	4.00±0.00	0.002±0.001	0.999
pH 9.0						
0.18	0.05	0.33±0.01	0.97	17.05±0.37	0.02±0.01	0.999
	0.10	0.56±0.01	0.88	16.70±0.62	0.09±0.01	0.999
	0.20	0.69±0.02	0.91	12.88±1.11	0.24±0.03	0.999
0.27	0.05	0.75±0.12	0.98	24.77±0.60	0.11±0.07	0.999
	0.10	0.90±0.08	0.97	16.52±1.64	0.18±0.13	0.999
	0.20	1.66±0.41	0.99	13.14±2.07	0.17±0.08	0.999
0.36	0.05	0.90±0.08	0.93	32.88±1.32	0.30±0.08	0.999
	0.10	1.23±0.04	0.98	16.54±1.38	0.19±0.05	0.999
	0.20	1.41±0.11	0.99	13.71±1.07	0.76±0.01	0.999

proceeds slower at higher catalyst loading. It should be noted that k_i has been normalize with respect to the catalyst loading and PMS dosage. This was also observed previously for the k_i values calculated from Eq. (10) in other heterogeneous PMS systems employing pseudo-first-order kinetics to model the pollutant degradation rate [14, 27]. This observation could be due to the fact that PMS activation by $CuFe_2O_3$-Fe_2O_3 is a multi-step activation process generating both $SO_4^{\bullet-}$ and $SO_5^{\bullet-}$ for BPA degradation (Eqs. (11)-(14)) [2, 22]:

$$Cu^{2+} + HSO_5^- \rightarrow Cu^{+} + SO_5^{\bullet-} + H^+ \quad (11)$$

$$Cu^{+} + HSO_5^- \rightarrow Cu^{2+} + SO_4^{\bullet-} + OH^- \quad (12)$$

$$Fe^{3+} + HSO_5^- \rightarrow Fe^{2+} + SO_5^{\bullet-} + H^+ \quad (13)$$

$$Fe^{2+} + HSO_5^- \rightarrow Fe^{3+} + SO_4^{\bullet-} + OH^- \quad (14)$$

The catalyst consists predominantly of transition metal at higher oxidation state (i.e. Cu^{2+} and Fe^{3+}) which favours the generation of $SO_5^{\bullet-}$ as the initial major activation steps (Eqs. (11)-(13)). When a higher catalyst loading is employed, a higher amount of PMS is instantaneously converted to $SO_5^{\bullet-}$ first for BPA oxidation resulting is less PMS available for producing $SO_4^{\bullet-}$. The $SO_5^{\bullet-}$ is a considerably weaker radical

View Article Online
DOI: 10.1039/C5TA06563A

than $SO_4^{\bullet-}$ which lowers the BPA degradation rate [13]. While the redox reaction also produces Fe^{2+} which is critical to generate $SO_4^{\bullet-}$, excessive Fe^{2+} generated from $SO_5^{\bullet-}$ production at higher catalyst loading acts as a strong quencher for $SO_4^{\bullet-}$ [28, 29]:

$$Fe^{2+} + SO_4^{\bullet-} \rightarrow Fe^{3+} + SO_4^{2-} \quad (k_{Fe^{2+}+SO4\bullet-} = 3 \times 10^8\ M^{-1}\ s^{-1}) \quad (15)$$

As such, it can be construed that at lower catalyst loading, the PMS can be utilized more efficiently to generated $SO_4^{\bullet-}$ for BPA degradation. All the k_i values at pH 9.5 are significantly higher than those at pHs 4.5 and 7.0 attributed to the production of $HO^{\bullet}$. At alkaline condition, synergistic BPA degradation by both $SO_4^{\bullet-}$ and $HO^{\bullet}$ occurs. No consistent trend for k_{PMS} was observed which could be due to the complex interaction of PMS with different generated radicals (e.g.: $SO_4^{\bullet-}$, $HO^{\bullet}$, $SO_5^{\bullet-}$ etc.) [29-31]. The PMS could also react with both the BPA and its intermediates.

$$HSO_5^- + SO_4^{\bullet-} \rightarrow SO_5^{\bullet-} + SO_4^{2-} + H^+ \quad (k_{HSO5^-+SO4\bullet-} = 1 \times 10^5\ M^{-1}\ s^{-1}) \quad (16)$$

$$HSO_5^- + HO^{\bullet} \rightarrow SO_5^{\bullet-} + SO_4^{2-} + H^+ \quad (k_{HSO5^-+OH\bullet} = 1 \times 10^7\ M^{-1}\ s^{-1}) \quad (17)$$

$$HSO_5^- + SO_5^{\bullet-} + H_2O \rightarrow SO_4^{\bullet-} + SO_4^{2-} + O_2 + H_3O^+ \quad (18)$$

$$HSO_5^- + SO_5^{\bullet-} + H_2O \rightarrow HO^{\bullet} + 2SO_4^{2-} + O_2 + 2H^+ \quad (19)$$

3.2.3 Effects of water matrix species

Fig. 8a shows the effects of various water matrix species (Cl^-, NO_3^-, HCO_3^-, PO_4^{3-} and HA) on BPA degradation. The kinetic model (Eq. 9) was used to describe BPA degradation rate in the presence of different water matrix species and their respective intrinsic rate constants, k_i (R^2>0.99), are presented in Fig. 8b. The concentrations of water matrix species were selected to resemble the typical characteristics of wastewater. The results indicated that Cl^- and HA exerted significant negative impact while the NO_3^-, HCO_3^- and PO_4^{3-} anions did not have significant impact on the BPA degradation. It is known that the Cl^- anion could quench the generated $SO_4^{\bullet-}$ to produce weaker radicals ($Cl^{\bullet}$ and $Cl_2^{\bullet-}$ as shown in Eqs. (20)-(21), respectively) and HClO [32, 33] while HA consume PMS and competes with BPA for the reactive $SO_4^{\bullet-}$ and PMS (Eqs. (22)-(23)) thus retarding the BPA degradation reaction. Moreover, HA could also foul the catalyst leading to the deactivation of the catalytic active sites for PMS activation [34].

$$Cl^- + SO_4^{\bullet-} \rightarrow Cl^{\bullet} + SO_4^{2-} \quad (k_{Cl^-+SO4\bullet-} = 2.8 \times 10^8\ M^{-1}\ s^{-1}) \quad (20)$$

$$Cl^- + Cl^{\bullet} \rightarrow Cl_2^{\bullet-} \quad (k_{Cl^-+Cl\bullet} = 8 \times 10^9\ M^{-1}\ s^{-1}) \quad (21)$$

$$\text{Humic acid} + HSO_5^- \rightarrow \text{by-products} + SO_4^{2-} \quad (22)$$

$$\text{Humic acid} + SO_4^{\bullet-} \rightarrow \text{by-products} + SO_4^{2-} \quad (23)$$

Previous report has indicated that PO_4^{3-} anion at natural pH can induce the formation of $SO_4^{\bullet-}$ from PMS which could have a positive effect on BPA degradation. However, a higher PO_4^{3-} concentration of up to 9 g L^{-1} than that used in this study (100 mg L^{-1}) was required to have a significant effect [35]. The HCO_3^- anion is a strong $SO_4^{\bullet-}$ and $OH^{\bullet}$ quencher (Eqs. (24)-(25)) and previous study has reported that it could induce detrimental effect to the BPA degradation rate but this was not observed in this study due to the use of a lower HCO_3^- concentration in this study [36].

$$HCO_3^- + SO_4^{\bullet-} \rightarrow SO_4^{2-} + CO_3^{\bullet-} + H^+ \quad (k_{HCO3^-/SO4\bullet-} = 1.6 \times 10^6\ M^{-1}\ s^{-1}) \quad (24)$$

$$HCO_3^- + OH^{\bullet} \rightarrow CO_3^{\bullet-} + H_2O \quad (k_{HCO3^-/OH\bullet} = 8.5 \times 10^6\ M^{-1}\ s^{-1}) \quad (25)$$

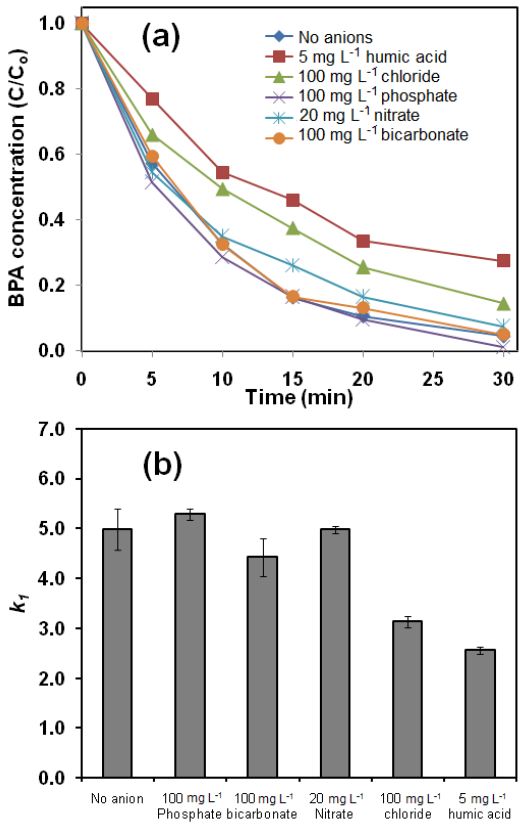

Fig. 8: (a) Effects of different water matrix species on the BPA degradation and (b) k_i values. Initial conditions: [pH] = 7.0±0.2, [PMS] = 0.18 g L^{-1}, [catalyst] = 0.05 g L^{-1}, and [BPA] = 5 mg L^{-1}.

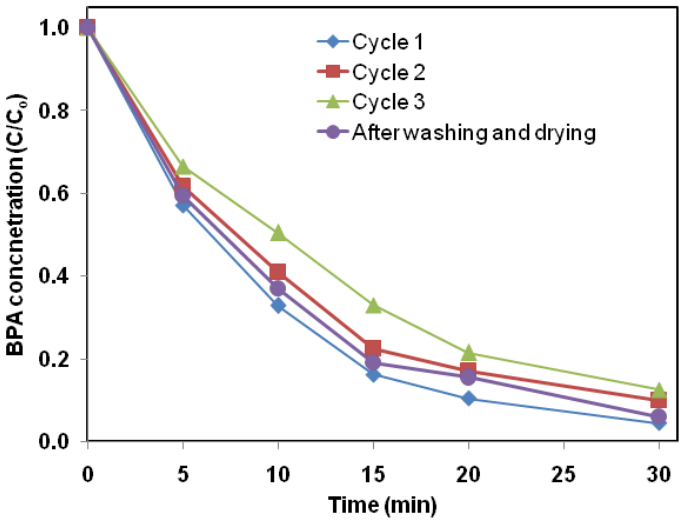

Fig. 9: Reusability of the $CuFe_2O_3$-Fe_2O_3 catalyst. Initial conditions: pH = 7.0±0.2, [PMS] = 0.18 g L^{-1}, [catalyst] = 0.05 g L^{-1}, and [BPA] = 5 mg L^{-1}.

3.3 Catalyst stability and reusability

Fig. 9 shows the reusability of $CuFe_2O_3$-Fe_2O_3 for BPA removal via PMS activation over 3 cycles. After 3 consecutive cycles, the rate of BPA removal rate decreased slightly. This could be due to the adsorption of BPA degradation intermediates on the catalyst surface, as evidenced by the presence of an additional absorbance band at 1000 cm^{-1} in the FTIR spectra of the used catalyst (Fig. 2g) which could be attributed to C-O stretching of the aromatic ring. The catalyst can be reused with no significant difference in the performance by simple washing and drying indicating that the low-temperature synthesis method could produce a stable, efficient and easily regenerable catalyst for generating $SO_4^{\bullet-}$ from PMS.

Conclusions

The $CuFe_2O_3$-Fe_2O_3 catalyst was successfully synthesized via an eco-friendly co-precipitation protocol at low temperature to generate sulfate radical from PMS for BPA removal. The mechanism of formation of $CuFe_2O_3$-Fe_2O_3 at low temperature is proposed. The $CuFe_2O_3$-Fe_2O_3 catalyst performed significantly better than other catalysts, namely ferrospinels (YFe_2O_4, Y = Cu, Co and Mn), Cu-based spinels (CuX_2O_4, X = Bi and Al) and Fe_2O_3 attributed to its preparation method without the use of organic precursors and efficient synergistic redox coupling between Cu^{2+} and Fe^{3+}. A kinetic model was developed based on the mechanistic consideration of the influences of various operating parameters, namely pH, PMS dosage and catalyst loading. The proposed mechanistic kinetic model fitted relatively better than the pseudo-first order kinetics, which did not take into consideration the pH-dependent surface-charge effect. The relationship between the pseudo first-order rate constant (k_{app}) and the intrinsic rate constant, (k_i) was established. The presence of chloride and humic acid in the solution could significantly affect the BPA degradation rate. This work provides new insights into the use of environmentally-benign catalyst for efficient degradation of the xenobiotic pollutants via sulfate radicals-based advanced oxidation processes.

Acknowledgements

The financial support from Academic Research Fund RG76/12 is gratefully acknowledged. The authors would also like to the interdisciplinary graduate school (IGS) and Nanyang Environment and Water Research Institute (NEWRI) for the award of PhD research Scholarship. The kind assistances from all the technical staffs in the Environmental Labs are deeply appreciated.

References

[1] G.P. Anipsitakis, D.D. Dionysiou, M.A. Gonzalez, Environmental Science & Technology, 2005, **40**, 1000.
[2] W.-D. Oh, S.-K. Lua, Z. Dong, T.-T. Lim, Journal of Hazardous Materials, 2015, **284**, 1.
[3] G.P. Anipsitakis, D.D. Dionysiou, Environmental Science & Technology, 2004, **38**, 3705.
[4] Y. Hardjono, H. Sun, H. Tian, C.E. Buckley, S. Wang, Chemical Engineering Journal, 2011, **174**, 376.
[5] Z. Huang, H. Bao, Y. Yao, W. Lu, W. Chen, Applied Catalysis B: Environmental, 2014, **154–155**, 36.
[6] Y. Ding, L. Zhu, N. Wang, H. Tang, Applied Catalysis B: Environmental, 2013, **129**, 153.
[7] T. Zhang, H. Zhu, J.-P. Croué, Environmental Science & Technology, 2013, **47**, 2784.
[8] F. Ji, C. Li, L. Deng, Chemical Engineering Journal, 2011, **178**, 239.
[9] F. Ji, C. Li, Y. Liu, P. Liu, Separation and Purification Technology, 2014, **135**, 1.
[10] J.I. Eid, S.M. Eissa, A.A. El-Ghor, The Journal of Basic & Applied Zoology, 2015, **71**, 10.
[11] J.R. Rochester, Reproductive Toxicology, 2013, **42**, 132.
[12] T. Olmez-Hanci, D. Dursun, E. Aydin, I. Arslan-Alaton, B. Girit, L. Mita, N. Diano, D.G. Mita, M. Guida, Chemosphere, Supplement (2015), **119**, S115.
[13] W.-D. Oh, S.-K. Lua, Z. Dong, T.-T. Lim, Journal of Materials Chemistry A, 2014, **2**, 15836.
[14] J. Liu, Z. Zhao, P. Shao, F. Cui, Chemical Engineering Journal, 2015, **262**, 854.
[15] J. Zhang, X. Shao, C. Shi, S. Yang, Chemical Engineering Journal, 2013, **232**, 259.
[16] F. Qi, W. Chu, B. Xu, Chemical Engineering Journal, 2014, **235**, 10.
[17] B.K. Kwak, D.S. Park, Y.S. Yun, J. Yi, Catalysis Communications, 2012, **24**, 90.
[18] H. Deng, H. Chen, H. Li, Materials Chemistry and Physics, 2007, **101**, 509.
[19] Y. Yao, Y. Cai, F. Lu, F. Wei, X. Wang, S. Wang, Journal of Hazardous Materials, 2014, **270**, 61.
[20] M.V. Lopez-Ramon, F. Stoeckli, C. Moreno-Castilla, F. Carrasco-Marin, Carbon, 1999, **37**, 1215.
[21] J. Li, J. Zhu, X. Liu, Dalton Transactions, 2014, **43**, 132-137.
[22] Y. Ren, L. Lin, J. Ma, J. Yang, J. Feng, Z. Fan, Applied Catalysis B: Environmental, 2015, **165**, 572.
[23] W. Zhang, H.L. Tay, S.S. Lim, Y. Wang, Z. Zhong, R. Xu, Applied Catalysis B: Environmental, 2010, **95**, 93.
[24] Y.-H. Guan, J. Ma, Y.-M. Ren, Y.-L. Liu, J.-Y. Xiao, L.-q. Lin, C. Zhang, Water Research, 2013, **47**, 5431.
[25] Z.-T. Hu, B. Chen, T.-T. Lim, RSC Advances, 2014, **4**, 27820.
[26] X. Chen, W. Cai, C. Fu, H. Chen, Q. Zhang, J Sol-Gel Sci Technol, 2011, **57**, 149.
[27] C. Tan, N. Gao, Y. Deng, J. Deng, S. Zhou, J. Li, X. Xin, Journal of Hazardous Materials, 2014, **276**, 452.
[28] A. Rastogi, S.R. Al-Abed, D.D. Dionysiou, Applied Catalysis B: Environmental, 2009, **85**, 171.
[29] C. Brandt, R. Van Eldik, Chemical Reviews, 1995, 95, 119.
[30] O. Gimeno, J. Rivas, M. Carbajo, T. Borralho, WORLD, 2009, **57**, 223.

View Article Online
DOI: 10.1039/C5TA06563A

[31] T. Balakrishnan, S.D. Kumar, Journal of Chemical Sciences, 2000, **112**, 497.
[32] W.-D. Oh, S.-K. Lua, Z. Dong, T.-T. Lim, Nanoscale, 2015, **7,** 8149.
[33] P. Wang, S. Yang, L. Shan, R. Niu, X. Shao, Journal of Environmental Sciences, 2011, **23**, 1799.
[34] B.P. Chaplin, E. Roundy, K.A. Guy, J.R. Shapley, C.J. Werth, Environmental Science & Technology, 2006, **40**, 3075.
[35] X. Lou, L. Wu, Y. Guo, C. Chen, Z. Wang, D. Xiao, C. Fang, J. Liu, J. Zhao, S. Lu, Chemosphere, 2014, **117**, 582.
[36] J. Sharma, I.M. Mishra, D.D. Dionysiou, V. Kumar, Chemical Engineering Journal, 2015, **276**, 193.